

# Thomson scattering density calibration by Rayleigh and rotational Raman scattering on NSTX<sup>a)</sup>

B. P. LeBlanc<sup>b)</sup>

*Princeton Plasma Physics Laboratory, Princeton, New Jersey 08543, USA*

(Presented 13 May 2008; received 10 May 2008; accepted 17 May 2008; published online 31 October 2008)

The multipoint Thomson scattering diagnostic measures the profiles of the electron temperature  $T_e(R)$  and density  $n_e(R)$  on the horizontal midplane of NSTX. Normal operation makes use of Rayleigh scattering in nitrogen or argon to derive the density profile. While the Rayleigh scattering  $n_e(R)$  calibration has been validated by comparison to other density measurements and through its correlation with plasma phenomena, it does require dedicated detectors at the laser wavelength in this filter polychromator based diagnostic. The presence of dust and/or stray laser light precludes routine use of these dedicated spectral channels for Thomson scattering measurement. Hence it is of interest to investigate the use of Raman scattering in nitrogen for the purpose of density calibration since it could free up detection equipment, which could then be used for the instrumentation of additional radial channels. In this paper the viewing optics “geometrical factor” profiles obtained from Rayleigh and Raman scattering are compared. While both techniques agree nominally, residual effects on the order of 10% remain and will be discussed. © 2008 American Institute of Physics. [DOI: [10.1063/1.2956747](https://doi.org/10.1063/1.2956747)]

## INTRODUCTION

The multipoint Thomson scattering (MPTS) diagnostic provides the electron temperature and density profiles and line integrated density needed for the routine operation of NSTX.<sup>1</sup> In its current configuration it uses two 30 Hz Nd:YAG (yttrium aluminum garnet) lasers operating at the fundamental harmonic of 1064 nm. The laser beams travel on the horizontal midplane providing profile measurements spanning 92% of the major radius of the machine aperture. A spherical mirror optics collects the scattered light along the path of each laser and focuses it on 36 fiber bundles, 29 of which are instrumented with one or two filter polychromators, for a total of 30 radial channels presently operational. The scattering geometry corresponds to the arrangement frequently seen, where a linearly polarized laser beam has its electric field perpendicular to the scattering plane. The density calibration relies on laser scattering in gas. The filter arrangement of a subset of the polychromators permits detection of both Rayleigh and Raman scattering light in three separate spectral channels. An alignment of the laser beams with the collecting optics normally precedes the laser scattering calibration. A primary alignment is done using a reference helium-neon laser and fiber bundle back illumination; this work is usually done one or two months prior to start of plasma operation, when access to the vacuum vessel is possible. When the vessel is under vacuum, the collection optics and the Nd:YAG laser beams are moved in small steps in order to ascertain the stray laser light. About three weeks

prior to plasma operation a final alignment is performed by sending the two laser beams into the vessel, which has been filled with 50 Torr of nitrogen previously left overnight in order to let the dust settle. This alignment is based on Raman scattering because of its immunity to stray laser light. A Raman scattering calibration is immediately performed once the alignment is optimized. The vessel is then pumped down to 1.5 Torr and a Rayleigh scattering calibration is done. The pumping to reduce pressure from 50 to 1.5 Torr has been found usually not to stir up dust. Sometimes argon is also used for Rayleigh scattering calibration at a pressure of 1.5 Torr. A recent modification has been the installation of a polarizer on the viewing optics. The proper orientation has been verified using Raman scattering. The ratio of with- and without-polarizer signals matches the expected 4/7, when the insertion loss is included in the calculation.

We can see in Fig. 1 a part of the spectral calibration data for a polychromator that can detect both Rayleigh and Raman scattering light. The smooth curves correspond to the avalanche photodiode (APD), quantum efficiency multiplied by the polychromator/filter transmission,  $QT_p$ , and were obtained through a spectral scan of a wide-band light source. A calculation for anti-Stokes rotational Raman scattering cross section in units of  $10^{-31} \text{ cm}^{-2}/\text{sr}$  for nitrogen is overlaid.<sup>2,3</sup> Rayleigh scattering is indicated but goes off scale. In what follows we will assume that solely Rayleigh scattering contributes light to the 1064 nm channel since the Raman contribution is of the order of 0.5%. On the other hand Raman signal is easily detected in the 1058 and 1048 nm channels. Stokes rotational Raman scattering, which occurs at wavelengths longer than 1064 nm, is not shown in the figure.

<sup>a)</sup> Contributed paper, published as part of the Proceedings of the 17th Topical Conference on High-Temperature Plasma Diagnostics, Albuquerque, New Mexico, May 2008.

<sup>b)</sup> Electronic mail: leblanc@pppl.gov.

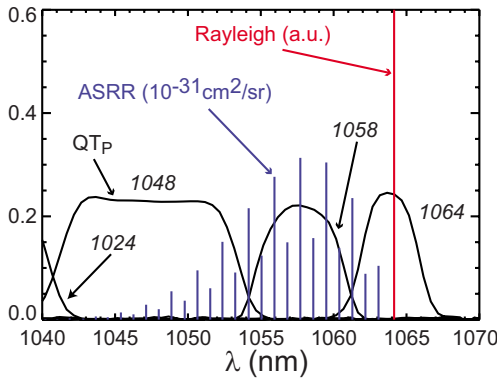


FIG. 1. (Color online) Overlay against wavelength of  $QT_p$  spectral calibration, cross section of anti-Stokes rotational Raman scattering lines and Rayleigh scattering line.

**GLOBAL GEOMETRIC FACTOR**

If one writes down the equations needed to calculate the signal resulting from Rayleigh, Raman or Thomson scattering, one finds a common factor of the form  $G = \Delta L \Delta \Omega T_C$ . This global geometry factor parameter, which is needed for the evaluation of the local electron density measured by Thomson scattering, folds in the details of the alignment of a laser beam with the viewing optics:  $\Delta L$  is the beam path observed,  $\Delta \Omega$  is the solid angle of light collection, and  $T_C$  is the transmission coefficient of the collecting optics. The  $G$  profile is a function of major radius  $R$  and is different for each laser. Based on Rayleigh scattering one finds

$$G = \Delta L \Delta \Omega T_C(\lambda_{Ry}) = \frac{\nu_{Ry} C_{fb}}{\left(\frac{d\sigma}{d\Omega}\right)_{Ry} n_{Ry} \frac{E_l}{hc} \lambda_{Ry} (QT_p)_{Ry} Meg} \tag{1}$$

Here  $\lambda_{Ry}$  is the scattering wavelength, which for Rayleigh scattering is the laser wavelength  $\lambda_{1064}$  of 1064 nm,  $(QT_p)_{Ry}$  corresponds to  $QT_p$  evaluated at  $\lambda_{Ry}$ ,  $\nu_{Ry}$  is the fast electronic signal,  $C_{fb}$  is the effective feedback capacitance of the transimpedance amplifier,  $(d\sigma/d\Omega)_{Ry}$  is the differential cross section,  $n_{Ry}$  is the gas density,  $E_l$  is the laser pulse energy,  $M$  is the APD gain,  $g$  is the fast electronics gain,  $e$  is the electron charge,  $h$  is Planck’s constant, and  $c$  is the speed of light in vacuum. More information about the MPTS detection electronics can be found elsewhere.<sup>4</sup> Similarly one finds the following expression for the evaluation of  $G$  from Raman scattering measurement:

$$G = \Delta L \Delta \Omega \overline{T_C(\lambda_{Rmj})} = \frac{\nu_{Rm} C_{fb}}{\left[ \sum_j F_j \left(\frac{d\sigma}{d\Omega}\right)_{Rmj} \lambda_{Rmj} (QT_p)_{Rmj} \right] n_{Rm} \frac{E_l}{hc} Meg} \tag{2}$$

Here  $\lambda_{Rmj}$  is the wavelength of anti-Stokes Raman lines,  $(QT_p)_{Rmj}$  corresponds to  $QT_p$  evaluated at  $\lambda_{Rmj}$ ,  $(d\sigma/d\Omega)_{Rmj}$  are the corresponding cross sections,  $n_{Rm}$  is the gas density, and  $\nu_{Rm}$  is the fast electronic signal.  $F_j$  is the fraction of the molecule density<sup>3</sup> that is in the upper state responsible for rotational line  $j$ . Raman scattering measurements of  $G$  can be made with the 1058 and 1048 nm spectral channels.

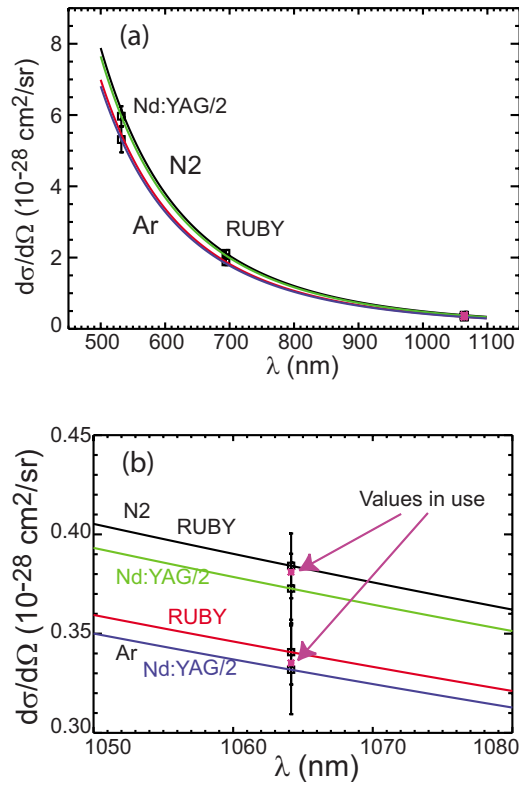


FIG. 2. (Color online) (a) Published measurements of Rayleigh scattering cross section for  $N_2$  and Ar at frequency doubled Nd:YAG laser and ruby laser wavelength. Extrapolation to Nd:YAG fundamental 1064 nm; (b) expanded view in the vicinity of 1064 nm.

**RAYLEIGH SCATTERING**

Since, somewhat surprisingly, the author was not able to find a published measurement of the Rayleigh cross section for nitrogen or argon at 1064 nm, estimates were made based on published data at lower wavelengths, by extrapolating to 1064 nm using the familiar  $1/\lambda^4$  scaling. Figure 2(a) shows such scalings based on measurements for nitrogen and argon done by Snee and Ubachs<sup>5</sup> at 532 nm—frequency doubled Nd:YAG laser—and by Rudder and Bach<sup>6</sup> done at 694.3 nm—ruby laser. The data published by Snee and Ubachs are the total Rayleigh cross section, which was converted to differential cross section using<sup>7</sup>

$$\left(\frac{d\sigma}{d\Omega}\right)_{Ry} = \frac{3\sigma}{8\pi} \left(\frac{2-\rho_0}{2+\rho_0}\right), \tag{3}$$

where  $\rho_0$  is the induced depolarization fraction for natural incident light. The latter was calculated based on the expression<sup>7</sup>  $F_k(\lambda) = (6+3\rho_0)/(6-7\rho_0)$ , where  $F_k$  is King’s correction factor<sup>8</sup> and making use of a functional for  $F_k(\lambda)$  derived by Bates<sup>9</sup> for nitrogen. One finds  $\rho_0 = 0.02$  for nitrogen. The depolarization fraction for argon is zero. The differential cross section at 1064 nm was computed using

$$(d\sigma/d\Omega)_{1064} = (d\sigma/d\Omega)_{\lambda_{exp}} (\lambda_{exp}/\lambda_{1064})^4. \tag{4}$$

The differential cross sections mentioned above at  $\lambda_{exp}$  of 532 and 694.3 nm for nitrogen and argon are shown in Fig. 2(a). Four curves based on Eq. (4) are overlaid and the extrapolated values at 1064 nm are also shown. Figure 2(b) shows an expanded view in the vicinity of 1064 nm. The

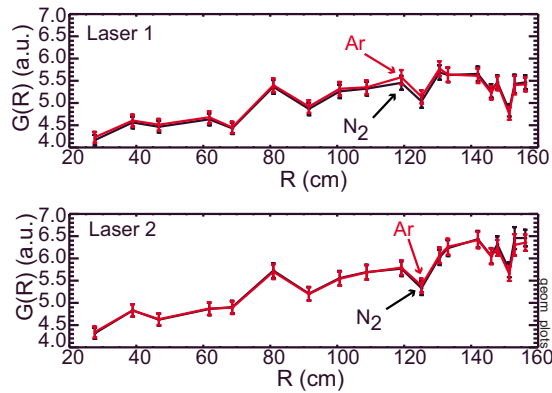


FIG. 3. (Color online) Overlay of  $G(R)$  measured by Rayleigh scattering in  $N_2$  and Ar: laser 1 on top panel, laser 2 at bottom panel. Measurements made at 1064 nm.

current values used by the MPTS system are indicated by asterisks. The two top curves correspond to nitrogen and are marked Nd:YAG/2 or ruby to indicate the measurement used for the extrapolation. Similar labeling is used for the two bottom curves, which correspond to argon. The errors at 1064 nm are scaled according to the experimental data. One can see that the differential cross sections in use for nitrogen and argon are within the error bars of the extrapolated data.

Figure 3 shows results from density calibrations based on Rayleigh scattering in nitrogen and argon; Eq. (1) was used to compute the  $G(R)$  factor profile against the major radius  $R$  for each laser. The top panel displays results obtained with laser 1 and the bottom panel shows the results for laser 2. One sees that the  $G(R)$  profiles obtained with nitrogen and argon agree within the error bar for each laser. Details of the laser beam profiles and the relative precision of the alignment explain the differences between the  $G(R)$  profiles obtained with each laser. On the other hand many of the  $G(R)$  features are common to both lasers, indicating that their origin lies within the collection optics and the detection hardware.

## RAMAN SCATTERING

It is of interest to ascertain whether the same level of confidence can be obtained with  $G$  profile calculation based on Raman scattering using Eq. (2). The relative intensity of the anti-Stokes Raman lines is proportional<sup>2</sup> to  $F_j(d\sigma/d\Omega)_{Rmj}$ , where

$$\left(\frac{d\sigma}{d\Omega}\right)_{Rmj} = \frac{64\pi^4}{45} \frac{3J(J-1)}{2(2J+1)(2J-1)} \frac{1}{\lambda_{Rmj}^4} \gamma^2. \quad (5)$$

Here  $J$  is the angular momentum quantum number and  $\gamma^2$  is the square of the nitrogen molecule polarizability anisotropy. The  $\gamma^2$  value for nitrogen has been measured at wavelengths lower than 1064 nm and a theoretical estimate has been made at 632.8 nm. Based on this information, McCool extrapolated<sup>3</sup>  $\gamma_{694}^2$  to  $0.45 \times 10^{-48} \text{ cm}^6$  at the ruby laser wavelength 694.3 nm. In this work, an experimental estimate of  $\gamma_{1064}^2$  at 1064 nm is done by solving  $\langle G(R, 1048, \gamma^2) \rangle = \langle G(R, 1064) \rangle$ , where the angle brackets indicate average over the major radius. This task is done by inserting Eq. (5) into Eq. (2) and varying  $\gamma^2$  in order to minimize  $S(\gamma^2)$

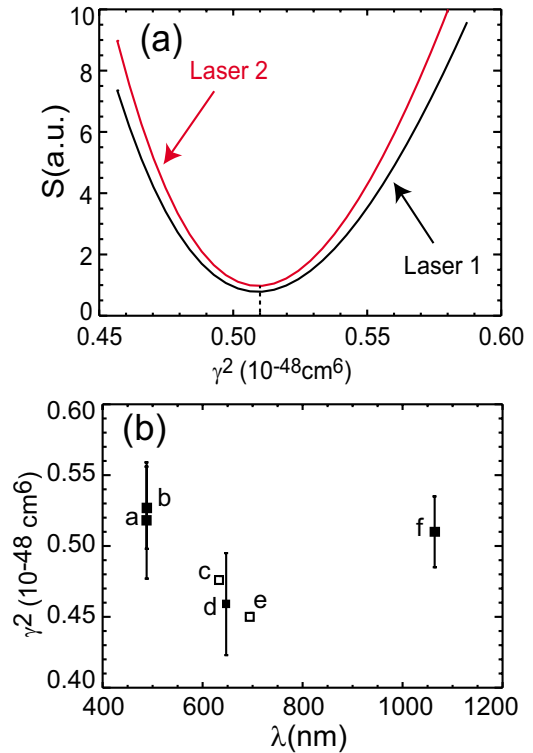


FIG. 4. (Color online) (a) Evaluation of square of nitrogen polarizability anisotropy  $\gamma^2$  at 1064 nm using data from lasers 1 and 2. (b) Published and measured values of  $\gamma^2$  against wavelength: a, c, d from Ref. 2, b from Ref. 10, e from Ref. 3; f, present estimate at 1064 nm.

$= \sum_n [G(R_n, 1048, \gamma^2) - G(R_n, 1064)]^2$ , where the summation is done over the major radial positions. One can see in Fig. 4(a) a plot of  $S$  against  $\gamma^2$ , where a well localized minimum occurs at the same  $\gamma^2$  for both lasers. A value of  $\gamma_{1064}^2 = (0.51 \pm 0.025) \times 10^{-48} \text{ cm}^6$  is obtained. Figure 4(b) shows a plot of  $\gamma^2$  against  $\lambda$ , where published values are shown for different wavelengths: entries a, c, d from Ref. 2, entry b from Buldakov *et al.*,<sup>10</sup> and e the extrapolation from Ref. 3. The data point f corresponds to the  $\gamma_{1064}^2$  experimental estimate described above for  $\lambda = 1064 \text{ nm}$ . Figure 5 shows three  $G$  profile measurements for each laser: (1) the profile marked 1064 was obtained with Rayleigh scattering; (2) the profile marked 1058 was obtained with Raman scattering and corresponds to data obtained through the 1058 nm spectral channels.

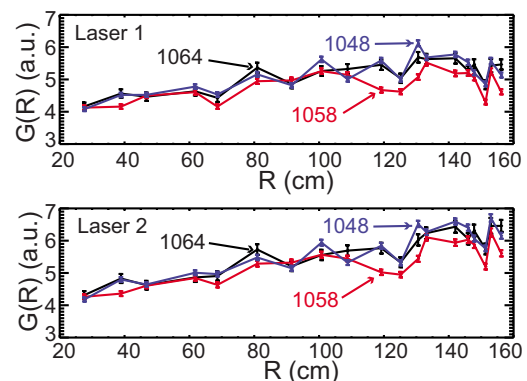


FIG. 5. (Color online) Overlay of  $G(R)$  measured by Raman and Rayleigh scattering in  $N_2$ : laser 1 on top panel, laser 2 at bottom panel. Measurements made with the 1048, 1058, and 1064 nm spectral channels.

1); (3) the profile marked 1048 was also obtained with Raman scattering and corresponds to data obtained from the 1048 nm filter. One can see that there is a good match between the 1064 and 1048 nm  $G(R)$  profiles throughout the major radius span. The 1058 nm  $G(R)$  profile does not match as well, particularly in the high major radius region. This can be explained by the fact that the 1064 and 1048 nm filters are located on the same side of the polychromator and their associated APD “sees” an unfocussed image of the fiber bundle end, while the APD associated with the 1058 nm filter sees a real image of the output end of the fiber bundle. Hence the 1064 and 1048 nm data constitute a better pair to match for the calculation of  $\gamma^2$ . The cause of the discrepancy between  $G(R,1058)$  and the matching  $G(R,1064)$  and  $G(R,1048)$  may be related to the radially varying etendue of MPTS’s backscattering geometry,<sup>11</sup> and could come from the  $QT_P$  calibration procedure, which at the moment does not involve the collection optics. While it is important that the latter concern be resolved, the good match between  $G(R,1064)$  and  $G(R,1048)$  opens up the possibility of using Raman instead of Rayleigh scattering to determine  $G$ . Since the signal at 1064 nm is routinely ignored during Thomson scattering data analysis because of the presence of stray laser light and Mye scattering, one might consider reallocating this particu-

lar detection hardware for the instrumentation of unused fiber bundles and hence increase the spatial resolution of the full system.

## ACKNOWLEDGMENTS

This work was supported by United States Department of Energy Contract No. DE-AC02-76CH03073.

- <sup>1</sup>B. P. LeBlanc, R. E. Bell, D. W. Johnson, D. E. Hoffman, D. C. Long, and R. W. Palladino, *Rev. Sci. Instrum.* **74**, 1659 (2003).
- <sup>2</sup>C. M. Penney, R. L. St. Peters, and M. Lapp, *J. Opt. Soc. Am.* **64**, 712 (1974).
- <sup>3</sup>St. C. McCool, Fusion Research Center, DOE/ET/53042-35, FRCR No. 242, 1982.
- <sup>4</sup>D. W. Johnson, B. P. LeBlanc, D. L. Long, and G. Renda, *Rev. Sci. Instrum.* **72**, 1129 (2001).
- <sup>5</sup>M. Sneep and W. Ubachs, *J. Quant. Spectrosc. Radiat. Transf.* **92**, 293 (2005).
- <sup>6</sup>R. R. Rudder and D. R. Bach, *J. Opt. Soc. Am.* **58**, 1260 (1968).
- <sup>7</sup>R. B. Miles, W. R. Lempert, and J. N. Forkey, *Meas. Sci. Technol.* **12**, R33 (2001).
- <sup>8</sup>L. V. King, *Proc. R. Soc. London, Ser. A* **104**, 333 (1923).
- <sup>9</sup>D. R. Bates, *Planet. Space Sci.* **32**, 785 (1984).
- <sup>10</sup>M. A. Buldakov, I. I. Matrosov, and T. N. Popova, *Opt. Spectrosc.* **46**, 488 (1979).
- <sup>11</sup>D. Johnson, N. Bretz, B. LeBlanc, R. Palladino, D. Long, and R. Parsells, *Rev. Sci. Instrum.* **70**, 776 (1999).